Appearance and disappearance of ferromagnetism in ultrathin LaMnO$_3$ on SrTiO$_3$ substrate: A viewpoint from first principles

Ming An, Yakui Weng, Huimin Zhang, Jun-Jie Zhang, Yang Zhang, and Shuai Dong[*]

School of Physics, Southeast University, Nanjing 211189, China

The intrinsic magnetic state (ferromagnetic or antiferromagnetic) of ultrathin LaMnO$_3$ films on the most commonly used SrTiO$_3$ substrate is a long-existing question under debate. Either strain effect or nonstoichiometry was argued to be responsible for the experimental ferromagnetism. In a recent experiment [X. R. Wang, C. J. Li, W. M. Lü, T. R. Paudel, D. P. Leusink, M. Hoek, N. Poccia, A. Vailionis, T. Venkatesan, J. M. D. Coey, E. Y. Tsymbal, Ariando, and H. Hilgenkamp, Science **349**, 716 (2015)], one more mechanism, namely, the self-doping due to polar discontinuity, was argued to be the driving force of ferromagnetism beyond the critical thickness. Here systematic first-principles calculations have been performed to check these mechanisms in ultrathin LaMnO$_3$ films as well as superlattices. Starting from the very precise descriptions of both LaMnO$_3$ and SrTiO$_3$, it is found that the compressive strain is the dominant force for the appearance of ferromagnetism, while the open surface with oxygen vacancies leads to the suppression of ferromagnetism. Within LaMnO$_3$ layers, the charge reconstructions involve many competitive factors and certainly go beyond the intuitive polar catastrophe model established for LaAlO$_3$/SrTiO$_3$ heterostructures. Our paper not only explains the long-term puzzle regarding the magnetism of ultrathin LaMnO$_3$ films but also sheds light on how to overcome the notorious magnetic dead layer in ultrathin manganites.

I. INTRODUCTION

Perovskite oxides in the form of ABO_3 are important materials, which cover a wide range of exotic physical properties including unconventional superconductivity, colossal magnetoresistance, multiferroicity, and so on [1–3]. Recent technical advances in film fabrications have enabled the atomic-level construction of various perovskite oxides and their heterostructures [4–9], which lead to new emergent physics at the interface/surface and shed light on potential electronic devices based on oxides [10–14]. By reducing the thickness and dimension, perovskites can exhibit distinct physical properties from the corresponding bulks, which are physically interesting and important for applications [15,16].

LaMnO$_3$ (LMO), as the parent compound of colossal magnetoresistance manganites [17], is one of the most studied perovskite oxides with abundant physical properties [18–20], and is also widely used as a building block in oxide heterostructures [21–34]. The bulk of LMO was reported to be A-type antiferromagnetic (A-AFM) at low temperatures, namely, spins are parallel in the ab plane but antiparallel between nearest neighbors along the c axis [17]. However, this A-AFM is quite fragile against tiny nonstoichiometry, and thus a sometimes obvious ferromagnetic (FM) signal is observed even for single crystalline samples [35]. In many experiments of LMO films on the most commonly used SrTiO$_3$ (STO) substrate, FM insulating behavior has been observed [22,32,34,36,37], which has been under debate for a long time. Both the strain effect and nonstoichiometry have been proposed to explain this A-AFM to FM transition [22,23,32,34,36–38].

Theoretically, many attempts suggest that the FM phase is intrinsic for STO-strained LMO [23,38–40]. For example,

double-exchange model calculations suggested the possible FM orbital-ordered (OO) phase for cubic LMO [23,41]. Based on density functional theory (DFT) calculations, Hou *et al.* proposed a new OO phase driven by strain as the FM insulating LMO [38]. Another recent DFT calculation by Lee *et al.* also claimed a FM phase for strained LMO although it was metallic [39].

Recently, Wang *et al.* synthesized high-quality epitaxial ultrathin LMO films on TiO$_2$ terminated [001]-oriented STO substrate and observed an atomically sharp transition from a no-magnetization phase to FM phase when the thickness of LMO reached five unit cells (u.c.) [42]. This thickness dependent magnetic transition was argued to be the result of charge reconstruction induced by polar discontinuity [42], since there was also a similar critical thickness in the polar catastrophe model for the (001)-orientated LaAlO$_3$/STO heterostructures [43–45]. This scenario, in which the FM phase is born from the intrinsic non-FM background due to the self-doping (i.e., electrons transfer from surface to interface), is in contradiction with aforementioned theoretical results [23,38,39]. However, if these theoretical calculations are correct, i.e., strained LMO film is intrinsically FM, it is a puzzle for the existence of a critical thickness in Wang *et al.*'s experiment, below which the FM signal disappears.

In fact, the disappearance of FM magnetization in ultrathin FM perovskite films, like doped manganite La$_{1-x}$Sr$_x$MnO$_3$ (LSMO) and SrRuO$_3$, is also a long-time puzzle with many debates [46–56]. This phenomenon is called magnetic "dead layers." The solution of magnetic dead layers is crucially important for the pursuit of magnetic oxide electronics. Therefore, as the first step, it is of particular importance to understand the physical mechanism of the thickness dependent magnetism in ultrathin magnetic perovskite films.

In this paper, the structural and magnetic properties of (001)-oriented vacuum/(LMO)$_n$/(STO)$_2$ heterostructures will be studied using DFT calculation, in order to reveal the

*Corresponding author: sdong@seu.edu.cn

mechanism behind the thickness dependent magnetic transition. It should be noted that, although there have been many DFT studies on strained LMO, some of these calculations have not really put STO layer and vacuum into consideration [38–40], or those previous DFT methods would fail to correctly describe the strain effect in LMO/STO heterostructures [57,58], as clarified in the following section. In addition, the $(LMO)_n/(STO)_m$ superlattices without surface will also be calculated. The comparison between these two series of LMO/STO heterostructures can highlight the vital role of the surface to magnetic phase transition in ultrathin LMO.

II. MODEL AND METHOD

LMO is a Mott insulator with the orthorhombic $Pbnm$ structure [18], as shown in Fig. 1(a). STO is a band insulator with a cubic perovskite lattice, the lattice constant (a_{STO}) of which is about 3.905 Å. The STO substrate provides a compressive strain ($\sim -2\%$) for the LMO film.

In the following, two series of LMO/STO heterostructures will be studied as sketched in Figs. 1(b) and 1(c). The first series is composed of superlattices constructed as $(LMO)_n/(STO)_m$ ($n = 1, 2, 3, 4, 5$; $m = 1, 2, 3$), in which atoms are periodically stacked along the [001] direction without surface. The second series is constructed as $(LMO)_n/(STO)_2$ ($n = 1, 2, 3, 4, 5$) with open surface (simulated by inserting a 15-Å vacuum layer). For the open surface heterostructures, the TiO_2 termination at the interface is adopted, considering the experimental practice [42].

To mimic the epitaxial stain from substrate STO, the in-plane lattice constants are fixed as $a = b = \sqrt{2}a_{STO} = 5.5225$ Å for both superlattices and open-surface heterostructures. The out-of-plane lattice constant c and the ionic coordinates are fully relaxed to reach the equilibrium state. For the open surface ones, the bottom atom layer of STO substrate (i.e., SrO) is fixed during the relaxation to mimic a very thick substrate. Thicker STO layers have also been checked, which do not change the conclusion (see Supplemental Material for

FIG. 1. Crystalline structures. (a) LMO bulk. (b) $(LMO)_2/(STO)_2$ superlattice. (c) $(LMO)_2/(STO)_2$ heterostructure with open surface. Here the TiO_2 layer is the interfacial termination and thus MnO_2 is the surface termination.

more details [59]). Therefore, two STO layers with fixed bottom are enough to simulate the substrate, which will be adopted in the following calculations.

First-principles calculations based on DFT are performed using the generalized gradient approximation [60] with the Perdew-Burke-Ernzerhof functional modified for solids (PBEsol) parametrization as implemented in the Vienna *ab initio* simulation package (VASP) [61–64]. The on-site Coulomb corrections U and J are applied to Ti's and Mn's $3d$ orbitals, the values of which have been systematically tested to reproduce the experimental lattice parameters and magnetic properties of bulk STO and LMO (see Supplemental Material for more details [59]). The U and J on La's $4f$ electrons have also been tested, which do not affect the physical results of LMO and thus will be neglected in the following calculations. The plane-wave cutoff energy is set to be 500 eV. The Γ-centered k-point meshes are set to be $7 \times 7 \times 5$ and $11 \times 11 \times 11$ for LMO and STO bulks, respectively, while $5 \times 5 \times 2$ mesh and $5 \times 5 \times 1$ mesh are accordingly adapted for LMO/STO heterostructures. The atomic positions are optimized iteratively until the Hellmann-Feynman force on each atom is less than 0.01 eV/Å during structural relaxation. The dipole moment correction is also tested for heterostructures with open surfaces. However, this item only slightly affects the energy of our system and does not change any physical conclusions.

III. RESULTS

A. Tests of LMO and STO

Before the simulation of heterostructures, it is essential to check the physical properties of LMO and STO bulks, which is not a trivial task [38,65–69].

First, it is well known that the magnetic ground state of LMO is difficult to capture in DFT calculations [42,65,66]. If the frequently used Dudarev implementation [70] is adopted to apply $U_{eff}(=U - J)$, the ground state is always the FM after the structure relaxation, despite the value of U_{eff} and the choice of pseudopotentials (PBE or PBEsol), as shown in Fig. 2(a). This bias to FM was repeatedly reported by previous literature [42,65,66], and sometimes artificial energy compensation was used to move the phase boundary [42]. However, such artificial operation makes it not convincing to predict new physics or understand the correct physical mechanism.

Second, there are other methods to obtain the A-AFM for LMO. For example, Hou *et al.* [38] used the PW91 pseudopotentials and rotationally invariant LSDA+U introduced by Liechtenstein *et al.* [71]. And Lee *et al.* used PBE pseudopotentials and also the Liechtenstein method to apply U and J [39]. Both these calculations can lead to the A-AFM ground state. However, their choices will lead to large deviation for the STO lattice constant, as shown in Fig. 2(d). Furthermore, in their calculations, the lattice constants of LMO did not precisely match the experimental ones either [see Fig. 2(c)]. Thus, there were uncertainties regarding the strain between STO and LMO layers in these calculations. These subtle deviations may obstruct the correct understanding of magnetism in LMO/STO heterostructures, since LMO itself is just staying at the edge of the phase boundary.
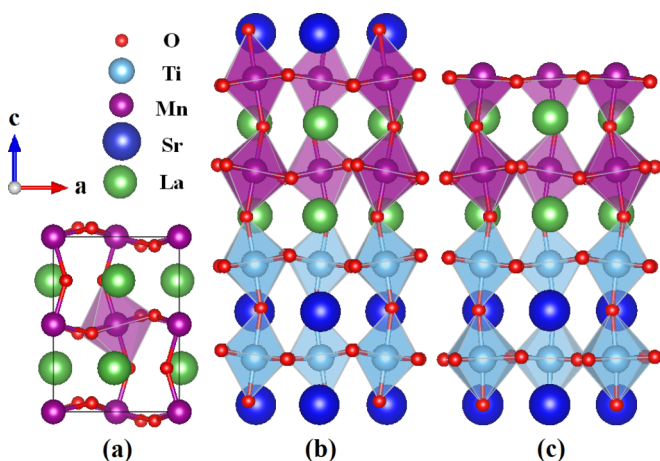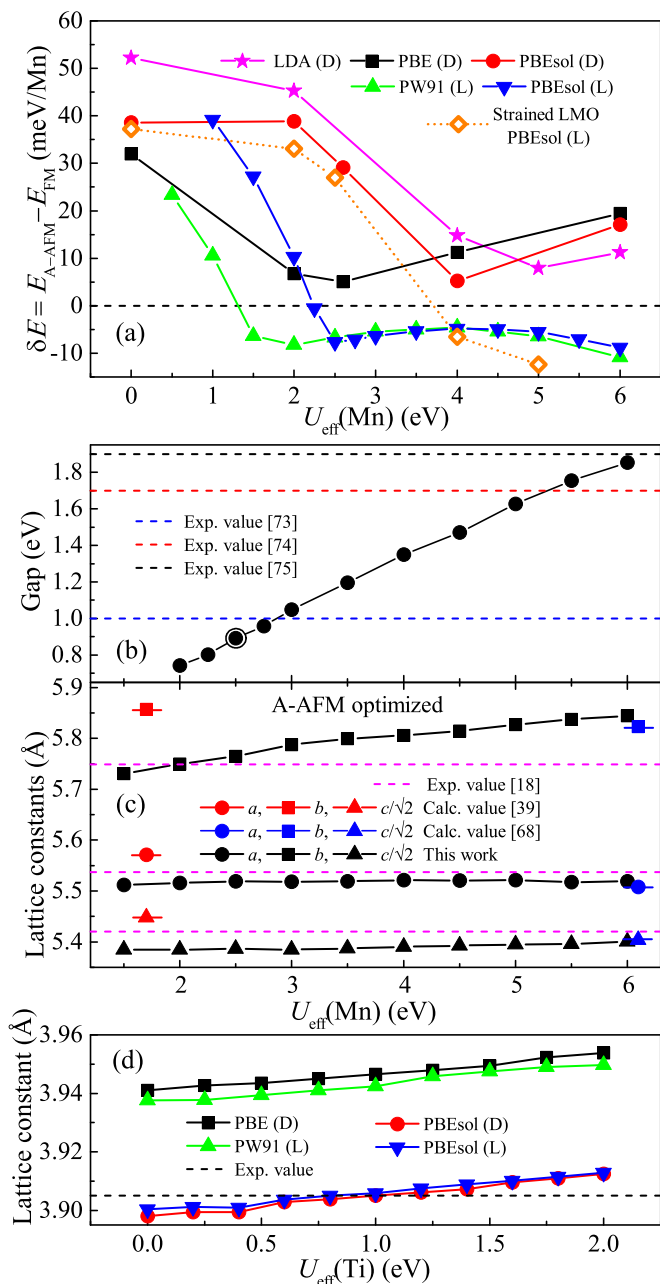
FIG. 2. (a) The energy difference between A-AFM and FM states for LMO bulk. Different pseudopotentials and adding-U methods have been compared. L, Liechtenstein's method; D, Dudarev's method. Other magnetic states (e.g., G-type AFM and C-type AFM) are also tested, which are much higher in energy and thus not shown here. The strained LMO case is also shown as the orange dashed curve. (b) The calculated band gap of bulk LMO with respect to different $U_{eff}(Mn)$. For comparison, several experimental values are also presented as dashed lines. (c) The optimized lattice constants of LMO for the A-AFM ground state. The experimental values [18,68] and previous DFT values [67] are shown for comparison. (d) The optimized lattice constant of cubic STO. Here $\frac{J(Mn)}{U(Mn)}$ is fixed as 0.286, while $\frac{J(Ti)}{U(Ti)}$ is fixed as 0.273. More discussions on the choice of $\frac{J}{U}$ can be found in Supplemental Material [59].

Third, the newly developed PBEsol potentials can give much improved precision to describe the crystalline structure for bulks [72]. By using the Liechtenstein method to apply U/J and the PBEsol potentials, our structural optimization can properly reproduce the A-AFM ground state, and obtain very precise structural information for both LMO and STO, in proper U ranges, as shown in Fig. 2. For example, when $U(Mn) = 3.5$ eV and $J(Mn) = 1$ eV, our calculation gives A-AFM as the ground state, the energy of which is lower than the FM state for 7.8 meV/Mn. The deviations of lattice constants from low-temperature experimental values [18] are within -0.3, 0.4, and -0.6% for a, b, and c, respectively. And when $U(Ti) = 1.2$ eV and $J(Ti) = 0.4$ eV, the lattice constant of calculated STO is just 3.905 Å. These results pave the solid bases for the following calculations on LMO/STO heterostructures. Only the precise structures can correctly describe the strain within LMO/STO heterostructures. In this sense, our results on LMO and STO provide a reliable starting point to reveal the physical mechanism of magnetic transition. In the following, these U's and J's will be adopted by default.

In addition, the estimated local magnetic moment is about 3.6 μ_B per Mn, which is close to the expected high spin value [16,19].

The calculated band gap of LMO is shown in Fig. 2(b). Several experimental values from different groups are also presented for comparison [73–75]. Our chosen $U(Mn)$ and $J(Mn)$ lead to ∼0.9 eV, lower than all experimental values more or less. It is a well-known drawback that DFT calculations always underestimate band gaps, especially for correlated electron systems. In Ref. [68], a very large U ($U = 8$ eV, $J = 1.9$ eV) was adopted to reproduce the experimental band gap of LMO. However, such a large U is abnormal for LMO according to literature [38,39,65,66]. In fact, it is not physically meaningful to fit the experimental band gap by simply using overlarge U. Other methods like GW calculation can be adopted to deal with the issue of band gap.

When the in-plane compressive strain (from STO substrate) is imposed on LMO bulk, i.e., by fixing the in-plane lattice constants of LMO to match the STO one and then relaxing the c-axis and atomic positions, the FM phase is indeed stabilized over the original A-AFM phases in the reasonable U range, as shown by the orange curve in Fig. 2(a). With the aforementioned default $U(Mn)$ and $J(Mn)$, the energy difference is ∼26 meV/Mn. Our conclusion regarding the strain induced FM phase in LMO qualitatively agrees with previous first-principles studies [38–40], although the concrete energy differences are different.

B. LMO/STO heterostructures

In this subsection, the LMO/STO heterostructures with various thicknesses will be calculated. The curves of energy are shown in Fig. 3.

For a heterostructure with an open surface, when the LMO epitaxial film is only 1 u.c. thick (one LaO layer plus one MnO_2 layer), very interestingly, the magnetic ground state becomes C-type AFM, the energy of which is lower than the FM state for 10 meV/Mn. Significantly, we predict C-type AFM in a LMO monolayer. When the LMO film is 2 u.c. thick, the ground state becomes FM, as in the strained bulk, although
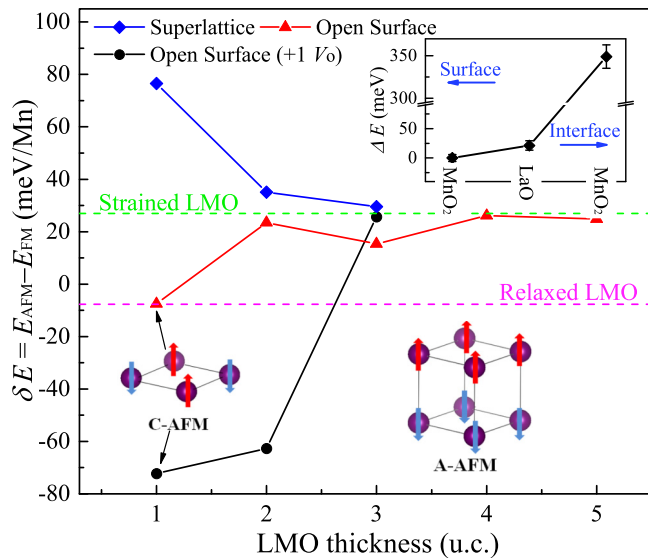
FIG. 3. Energy differences between two lowest magnetic states: in particular, C-type AFM and FM for $n = 1$ and A-AFM and FM for others. Other uniform magnetic orders such as C-type AFM are also calculated, which are much higher in energy. The energy differences between A-AFM and FM in unstrained and strained LMO bulks are also shown as dashed purple and green lines, respectively. Upper inset: the formation energy of one V_O as a function of layer positions in the $n = 2$ open surface case. The formation energy of V_O in the outmost layer is taken as the reference. Lower inset: sketch of C-type AFM and A-AFM.

FIG. 4. Total DOS (gray shaded area) and pDOS (color lines) of LMO/STO heterostructures. (a–e) $(LMO)_n/(STO)_2$ heterostructures with open surfaces. (f–h) $(LMO)_n/(STO)_n$ superlattices. The vertical dashed line denotes the Fermi level. (i) The DOS value (per Mn) at the Fermi level as a function of LMO thickness.

the energy difference between FM and AFM is a little lower than that of strained bulk. With further increasing thickness, as expected, the energy curve approaches the strained bulk gradually. In short, only the monolayer limit of MnO_2 becomes magnetically "dead" in our calculation, which does not fully agree with the experimental observation with the critical thickness of 5 u.c. [42].

For comparison, the $(LMO)_n/(STO)_n$ ($n = 1, 2, 3$) superlattices are also calculated, which shows clear FM tendency for all thickness. With increasing n, the energy curve also gradually approaches the strained LMO one. In fact, previous experiments on LSMO/STO superlattices indeed found that the strong FM magnetization could persist to the ultrathin limit (e.g., 4 or 5 u.c.) [51,52], while the LSMO films with open surfaces are much easier to be dead [49,50]. And many technical details, e.g., size of laser spots during the pulse laser deposition, can affect the magnetization of the LSMO layer [51], implying the crucial role of nonstoichiometry.

To trace the evolution of electronic structure, the density of states (DOS) and atom-projected DOS (pDOS) of LMO/STO heterostructures are exhibited in Fig. 4. In the series with an open surface, $(LMO)_1/(STO)_2$ exhibits an insulating behavior with a gap of ~1.1 eV. For thicker LMO, the heterostructures gradually become metallic, indicated by the enhanced DOS at Fermi level with increasing thickness [Fig 4(i)]. Although the experiment reported insulating behavior of ultrathin LMO of few layers [42], the discrepancy may be due to two reasons. First, as mentioned before, the band gaps are usually underestimated in DFT calculations. Second, the weak metallicity, i.e.,

small DOS values at Fermi level in our DFT calculations, can be easily suppressed in real materials due to intrinsic and extrinsic localizations. For comparison, the metallicity is much better in the $(LMO)_n/(STO)_n$ superlattice, always with relatively larger DOS values at Fermi level. The states of Ti are mostly above the Fermi level and thus empty. The charge transfer from Mn to Ti across the interface is evaluated by integrating the pDOS of Ti, which is only ~0.03 electron per interfacial Ti (a negligible value), consistent with previous reports [57,58].

In the experimental sample growth process of oxides, oxygen vacancies (V_O's) seem to be inevitable, more or less [34,76–80]. Therefore, it is interesting to check the role of oxygen vacancies. Here one oxygen vacancy site is considered in our calculation. First, the forming energies of various V_O's are calculated, which suggest the topmost V_O is the most probable one (see the inset of Fig. 3). By creating this V_O, the system indeed becomes more likely to be antiferromagnetic. For the monolayer with one V_O (16.7%), the C-AFM is lower in energy than the FM state for more than 70 meV/Mn. And for the bilayer of LMO with one V_O (8.3%), the A-AFM becomes the most stable one. Only starting from the trilayer of LMO with one V_O (5.6%), the FM one takes over the ground state. It is rather complicated to consider multiple V_O's in thick LMO films due to too many possible combinations of V_O sites as well as combinations of possible nonuniform magnetic orders, even though our results for the single V_O cases already qualitatively indicate that the oxygen deficiency at the surface is determinant for the disappearance of FM magnetization, namely, the magnetic dead layers.

The DOS and pDOS for heterostructures with one V_O are shown in Fig. 5. The most significant change is the impurity state created near the Fermi level, which is quite reasonable.
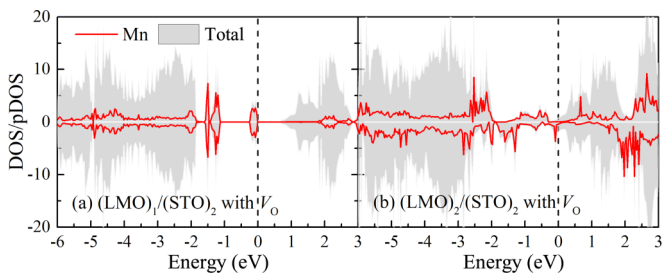
FIG. 5. The DOS and pDOS of Mn of nonstoichiometric (a) $(LMO)_1/(STO)_2$ and (b) $(LMO)_2/(STO)_2$ heterostructures, within which the surface oxygen is deficient.

In summary of our DFT results, the ferromagnetism of LMO is induced by the compressive strain from STO. The magnetic dead layers in ultrathin LMO film beyond monolayer are not intrinsic, but probably due to the oxygen vacancies near the surface.

IV. DISCUSSION

A. Charge redistribution and potential modulation

The polar discontinuity has been well recognized as the origin of two-dimensional electron "gas" in LaAlO$_3$/STO heterostructures [43,44,81]. In Ref. [42], the polar discontinuity of TiO$_2$ and LaO was argued to cause an electrostatic field, which led to charge redistribution. Wang *et al.* proposed that the FM tendency beyond the critical thickness in LMO layers was due to this self-doping effect, while LMO itself should be non-FM [42]. This scenario is different from our DFT result mentioned before. Thus, it is necessary to check the polar discontinuity effect using DFT calculations.

The on-site potential of MnO$_2$ layers can be estimated using oxygen 1s core-level energy, as shown in Figs. 6(a) and 6(b). First, the open surface cases show much larger modulation of potential, while the potential modulation in the superlattice is rather mild. In fact, polar discontinuity exists in both cases and should be similar in magnitude before charge-density redistribution. According to the calculated Bader charge for each MnO$_2$ layer [Figs. 6(c) and 6(d)], there is indeed an overall tendency for electron transfer to the interface. If this electron transfer from p-type interface (or surface) to n-type interface is stronger, the electrostatic potential can be largely compensated. However, by comparing Figs. 6(c) and 6(d), the charge redistribution is more significant in the open surface cases. In this sense, the mild potential modulations in superlattices cannot be attributed to the compensation by weak charge transfer.

Instead, the high dielectric constant of STO layers may compensate partial polar discontinuity in superlattices, as evidenced by the displacements of all Ti's along the same direction [see Fig. 6(a) for more details].

For all heterostructures, with or without open surfaces, there are clear charge-density oscillation along the c axis. This oscillation can be qualitatively understood as the effect from quantum confinement [33]. Such layer-dependent oscillation of electron density was once predicted in $(LMO)_n/(LaNiO_3)_n$ superlattices [33], but has rarely been reported in the LaAlO$_3$/STO case. In the LaAlO$_3$/STO case, the dominant
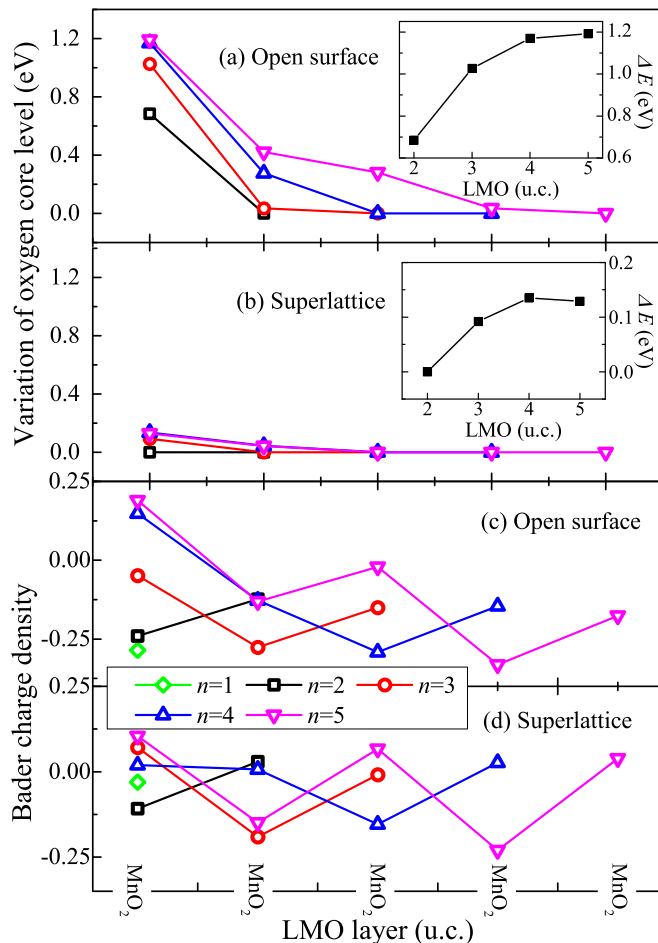
FIG. 6. Potential and electron density in LMO layers, counted from the surface or TiO$_2$-SrO-MnO$_2$ interface. (a, b) Energy profile of O's 1s orbital as a function of the MnO$_2$ layer index, which is an indication of on-site potential from electrostatic field over the heterostructures. The O in the interfacial MnO$_2$ layer is taken as the reference. (a) Superlattices. (b) Open surface cases. Insets: The potential difference (ΔE) between the top and bottom Mn's as a function of thickness. (c, d) Bader charge density of each MnO$_2$ layer. The reference density (value zero) is set as the Bader charge density for the MnO$_2$ layer in LMO bulk. Thus, a positive (negative) value means more electrons (holes) obtained. The oscillation of Bader charge density is very clear, while the unidirectional electron transfer from p-type interface (and surface) to n-type interface is obscure.

driving force for charge redistribution is the polar field from termination, making the electron distribution behave in a decaying manner from the interface. In contrast, there is no polar discontinuity in LaNiO$_3$/LMO, and thus the dominant effect is the quantum confinement, which makes the electron distribution behave in an oscillation manner. Here the LMO/STO cases are in the middle of these two limits. The polar discontinuity exists but is partially compensated by the many carriers in LMO layers. We note that the maximum number of electrons in $(LaAlO_3)_m/(STO)_n$ is 1, distributing over n layers of STO, while there are n e_g electrons distributed in n layers of LMO. Thus the polar discontinuity can be easily screened by one of these n electrons in the LMO/STO cases.
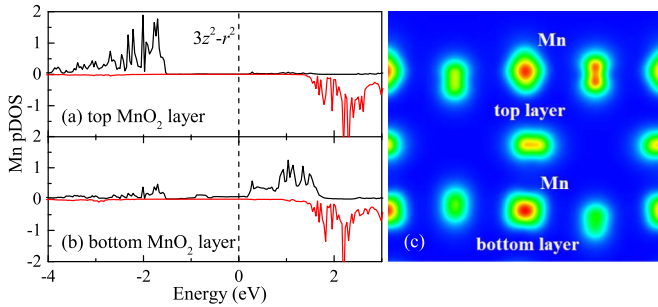
FIG. 7. Layer-resolved pDOS of the Mn $3z^2 - r^2$ orbital in (a) the top and (b) the bottom MnO_2 layer of vacuum/$(LMO)_2$/$(STO)_2$. (c) The electron density. The $3z^2 - r^2$ character is obvious for the top layer.

In addition, the interaction between the interfacial STO layer (or vacuum) and LMO also tuned the charge density near interface (surface) significantly. Especially for the open surface, the oxygen octahedra are broken, which can seriously change the crystalline filed of Mn's $3d$ orbitals. Thus, the energy of the $3z^2 - r^2$ orbital for the surface Mn is greatly reduced, attracting more electrons to the surface [82]. This conjecture can be further illustrated by the layer-resolved pDOS of Mn's $3z^2 - r^2$ orbital, as shown in Fig. 7.

In short, the potential modulation, as well as charge transfer in LMO layers, is driven by the collaborative effects of many issues, including polar discontinuity, dielectric screening of the STO layer, quantum confinement, as well as interface interactions (or broken octahedra at surface), which are rather complicated. Thus, the simplified model of polar catastrophe established for the LaAlO$_3$/STO system [44,81] cannot be directly applied to explain the LMO/STO heterostructures.

B. Structural modulation

In oxide heterostructures and films, the magnetism is usually related to the structural modulations [38,39,65]. To further understand the LMO/STO heterostructures, the layer-resolved structural information is presented in Fig. 8.

As stated in Sec. IV A, the polar discontinuity of the interface can be partially compensated by polar distortion of the STO layer. In fact, both STO and LMO layers are distorted to be polarized, as shown in Fig. 8(a). In all heterostructures, all Mn and Ti ions with positive charges move away from the TiO$_2$-LaO interface, as expected. Such polar distortions bend the in-plane O-Mn-O and O-Ti-O bond angles, which should be 180° in corresponding bulks. Such polar ferromagnetism was recently experimentally reported in LSMO/BaTiO$_3$ superlattices [83], which was attributed to be induced by ferroelectric distortion of BaTiO$_3$ [84]. Here in our studied system, the polar discontinuity of the interface can also induce polar ferromagnetism in ultrathin LMO layers. The displacement of each ion (Mn or Ti) from the average height of corresponding O$_2$ is plotted in Figs. 8(c) and 8(d). It is clear that the open surface leads to more significant polar distortion due to the broken octahedra. At least for this polar structural modulation, the surface effect is stronger than the interfacial effect.
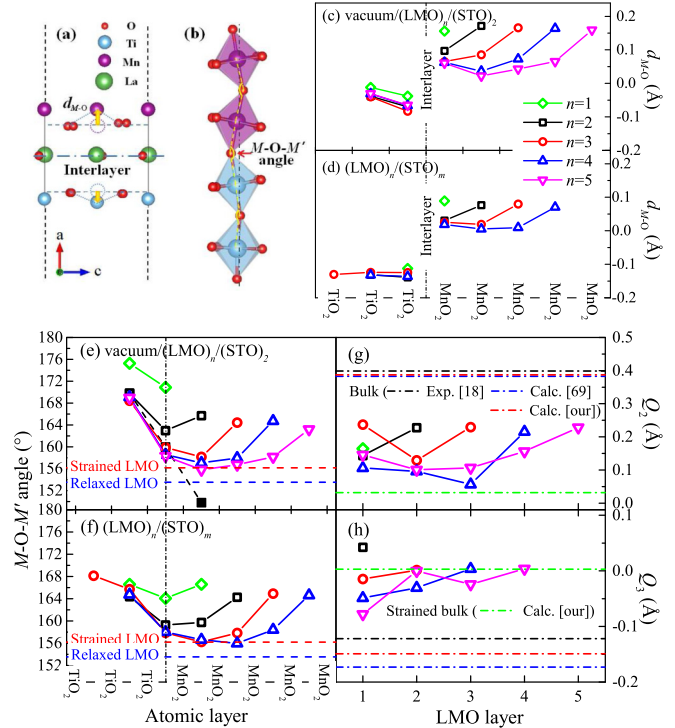
FIG. 8. Structural modulation in LMO/STO heterostructures. (a, b) Schematic of polar distortions and MO_6 octahedra tilting. (c, d) Polar distortions, characterized by the displacements of M, as a function of layer index. (e, f) M-O-M' bond angles along the c axis. All end points in panel (f) are Mn-O-Ti bonds. The case with a V_O is also shown in panel (e) as solid black dots. (g, h) The JT distortions in the LMO portion of vacuum/$(LMO)_n$/$(STO)_2$ heterostructures. For comparison, both the experimental and theoretical values for LMO bulks are also presented [18,69].

A recent experiment on LSMO/STO heterostructures revealed the layer dependent relaxation of MnO$_6$ octahedra tilting angles [85], which should make an important contribution to the magnetism. Generally, the tilting of octahedra bends Mn-O-Mn bonds, and thus changes the overlap between $3d$ and $2p$ orbitals, which tunes the exchange interactions. Here our DFT calculation can also provide the octahedra tilting evolution in ultrathin LMO layers. Figures 8(e) and 8(f) show the M-O-M' angles along the c direction for optimized heterostructures. In pure LMO bulk, the Mn-O-Mn bond angle along the c axis is 153°, which becomes straighter, 155°, due to the compressive strain in the strained case.

In heterostructures, due to the nontilting oxygen octahedra in the STO layer, the tilting of octahedra in LMO layers is suppressed more or less, depending on the distance from the interface. The Mn-O-Ti bond angles at the TiO$_2$-LaO-MnO$_2$ interface are mostly around 158° when LMO is beyond 2 u.c., while for the TiO$_2$-SrO-MnO$_2$ interface in superlattices the Mn-O-Ti bond angles are around 165°. The inner Mn-O-Mn bond is usually more bending closer to the intrinsic value of strained LMO, even though near the surface the Mn-O-Mn becomes straighter, all of which are larger than 162°. However, once a V_O is created at the surface, the out-of-plane Mn-O-Mn bond angle is significantly reduced to ~150°. Such V_O

enhanced distortions can strongly suppress the FM tendency [16,19], in agreement with the result presented in Fig. 3.

Besides the bending of bonds, the Jahn-Teller (JT) distortions also affect the properties of manganites [16,19,86]. The evolutions of JT modes (Q_2 and Q_3) in heterostructures with open surfaces are calculated, as shown in Figs. 8(g) and 8(h). For strained LMO bulk, the square geometry of the STO (001) plane strongly suppresses the Q_2 mode, while the compressive strain strongly suppresses the Q_3 mode. For the LMO/STO heterostructures, the values of Q_2 and Q_3 are between the two limits of unstrained and fully strained cases, more closer to the latter. Thus, the original $3x^2$-r^2/$3y^2$-r^2 orbital ordering should be generally suppressed, corresponding to the enhanced ferromagnetism. Especially, the Q_2 mode at the surface MnO_2 layer is largest.

In short, all these modulations of structural distortions suggest the crucial role of the surface.

V. SUMMARY

In the present paper, with carefully verified parameters, we have investigated through DFT calculations the physical properties of LMO and STO bulks, as well as strained LMO and LMO/STO superlattices. Our calculation indicates that the FM state is the ground state for ideally strained LMO on STO. Thus, the appearance of ferromagnetism is intrinsically driven by compressive strain. The disappearance of such ferromagnetism in ultrathin LMO of few layers on STO is mostly due to the open surface, which breaks the oxygen octahedra at the surface and leads to structural and electronic reconstruction. Furthermore, the outmost oxygen vacancies are more likely to be created, which significantly suppress the ferromagnetism. Thus nonstoichiometry effect should play an important role in the experimentally observed nonmagnetic state of ultrathin LMO films.

According to our calculations, the polar discontinuity of the interface can indeed induce charge redistribution near the LMO/STO interface, but it is not the decisive effect for either electron reconstruction or disappearance of magnetization. The polar structural distortion can partially compensate for the built-in electric field caused by polar discontinuity, making the self-doping effect weaker than expected.

Although our paper focused on LMO, the conclusion might be referential to understand and overcome the magnetic dead layers widely existing in FM oxide films.

[1] M. Imada, A. Fujimori, and Y. Tokura, Metal-insulator transitions, Rev. Mod. Phys. **70**, 1039 (1998).

[2] E. Dagotto, Complexity in strongly correlated electronic systems, Science **309**, 257 (2005).

[3] S. Dong, J.-M. Liu, S.-W. Cheong, and Z. F. Ren, Multiferroic materials and magnetoelectric physics: symmetry, entanglement, excitation, and topology, Adv. Phys. **64**, 519 (2015).

[4] D. G. Schlom, L.-Q. Chen, C.-B. Eom, K. M. Rabe, S. K. Streiffer, and J.-M. Triscone, Strain tuning of ferroelectric thin films, Annu. Rev. Mater. Res. **37**, 589 (2007).

[5] L. W. Martin, Y.-H. Chu, and R. Ramesh, Advances in the growth and characterization of magnetic, ferroelectric, and multiferroic oxide thin films, Mater. Sci. Eng. R **68**, 89 (2010).

[6] M. Bibes, J. E. Villegas, and A. Barthélémy, Ultrathin oxide films and interfaces for electronics and spintronics, Adv. Phys. **60**, 5 (2011).

[7] X. Huang and S. Dong, Ferroelectric control of magnetism and transport in oxide heterostructures, Mod. Phys. Lett. B **28**, 1430010 (2014).

[8] P. Zubko, S. Gariglio, M. Gabay, P. Ghosez, and J.-M. Triscone, Interface physics in complex oxide heterostructures, Annu. Rev. Condens. Matter Phys. **2**, 141 (2011).

[9] J. Chakhalian, A. J. Millis, and J. Rondinelli, Whither the oxide interface, Nat. Mater. **11**, 92 (2012).

[10] E. Dagotto, When oxides meet face to face, Science **318**, 1076 (2007).

[11] J. Mannhart and D. G. Schlom, Oxide interfaces: An opportunity for electronics, Science **327**, 1607 (2010).

[12] G. Hammerl and N. Spaldin, Shedding light on oxide interfaces, Science **332**, 922 (2011).

[13] H. Takagi and H. Y. Hwang, An emergent change of phase for electronics, Science **327**, 1601 (2010).

[14] H. Y. Hwang, Y. Iwasa, M. Kawasaki, B. Keimer, N. Nagaosa, and Y. Tokura, Emergent phenomena at oxide interfaces, Nat. Mater. **11**, 103 (2012).

[15] E. Dagotto, *Nanoscale Phase Separation and Colossal Magnetoresistance* (Springer, Berlin, 2002).

[16] Y. Tokura, Critical features of colossal magnetoresistive manganites, Rep. Prog. Phys. **69**, 797 (2006).

[17] E. O. Wollan and W. C. Koehler, Neutron diffraction study of the magnetic properties of the series of perovskite-type compounds [(1-x)La,xCa]MnO$_3$, Phys. Rev. **100**, 545 (1955).

[18] J. Rodríguez-Carvajal, M. Hennion, F. Moussa, A. H. Moudden, L. Pinsard, and A. Revcolevschi, Neutron-diffraction study of the Jahn-Teller transition in stoichiometric LaMnO$_3$, Phys. Rev. B **57**, R3189(R) (1998).

[19] E. Dagotto, T. Hotta, and A. Moreo, Colossal magnetoresistant materials: The key role of phase separation, Phys. Rep. **344**, 1 (2001).

[20] M. B. Salamon and M. Jaime, The physics of manganites: Structure and transport, Rev. Mod. Phys. **73**, 583 (2001).

[21] S. J. May, P. J. Ryan, J. L. Robertson, J.-W. Kim, T. S. Santos, E. Karapetrova, J. L. Zarestky, X. Zhai, S. G. E. te Velthuis, J. N. Eckstein, S. D. Bader, and A. Bhattacharya, Enhanced ordering temperatures in antiferromagnetic manganite superlattices, Nat. Mater. **8**, 892 (2009).

[22] A. Bhattacharya, S. J. May, S. G. E. te Velthuis, M. Warusawithana, X. Zhai, B. Jiang, J.-M. Zuo, M. R. Fitzsimmons, S. D. Bader, and J. N. Eckstein, Metal-Insulator Transition and

its Relation to Magnetic Structure in $(LaMnO_3)_{2n}/(SrMnO_3)_n$ Superlattices, Phys. Rev. Lett. **100**, 257203 (2008).

[23] S. Dong, R. Yu, S. Yunoki, G. Alvarez, J.-M. Liu, and E. Dagotto, Magnetism, conductivity, and orbital order in $(LaMnO_3)_{2n}/(SrMnO_3)_n$ superlattices, Phys. Rev. B **78**, 201102(R) (2008).

[24] C. Aruta, C. Adamo, A. Galdi, P. Orgiani, V. Bisogni, N. B. Brookes, J. C. Cezar, P. Thakur, C. A. Perroni, G. De Filippis, V. Cataudella, D. G. Schlom, L. Maritato, and G. Ghiringhelli, Evolution of magnetic phases and orbital occupation in $(SrMnO_3)_n/(LaMnO_3)_{2n}$ superlattices, Phys. Rev. B **80**, 140405(R) (2009).

[25] B. R. K. Nanda and S. Satpathy, Effects of strain on orbital ordering and magnetism at the perovskite oxide interfaces: $LaMnO_3/SrMnO_3$, Phys. Rev. B **78**, 054427 (2008).

[26] B. R. K. Nanda and S. Satpathy, Electronic and magnetic structure of the $(LaMnO_3)_{2n}/(SrMnO_3)_n$ superlattices, Phys. Rev. B **79**, 054428 (2009).

[27] H. Yamada, M. Kawasaki, T. Lottermoser, T. Arima, and Y. Tokura, $LaMnO_3/SrMnO_3$ interfaces with coupled charge-spin-orbital modulation, Appl. Phys. Lett. **89**, 052506 (2006).

[28] J. Garcia-Barriocanal, F. Y. Bruno, A. Rivera-Calzada, Z. Sefrioui, N. M. Nemes, M. Garcia-Hernández, J. Rubio-Zuazo, G. R. Castro, M. Varela, S. J. Pennycook, C. Leon, and J. Santamaria, Charge leakage at $LaMnO_3/SrTiO_3$ interfaces, Adv. Mater. **22**, 627 (2010).

[29] Q. F. Zhang, S. Dong, B. L. Wang, and S. Yunoki, Strain-engineered magnetic order in $(LaMnO_3)_n/(SrMnO_3)_{2n}$ super-lattices, Phys. Rev. B **86**, 094403 (2012).

[30] S. Dong, Q. F. Zhang, S. Yunoki, J.-M. Liu, and E. Dagotto, Magnetic and orbital order in $(RMnO_3)_n/(AMnO_3)_{2n}$ superlat-tices studied via a double-exchange model with strain, Phys. Rev. B **86**, 205121 (2012).

[31] W. S. Choi, D. W. Jeong, S. S. A. Seo, Y. S. Lee, T. H. Kim, S. Y. Jang, H. N. Lee, and K. Myung-Whun, Charge states and magnetic ordering in $LaMnO_3/SrTiO_3$ superlattices, Phys. Rev. B **83**, 195113 (2011).

[32] M. Gibert, P. Zubko, R. Scherwitzl, J. Íñiguez, and J.-M. Triscone, Exchange bias in $LaNiO_3 - LaMnO_3$ superlattices, Nat. Mater. **11**, 195 (2012).

[33] S. Dong and E. Dagotto, Quantum confinement induced mag-netism in $LaNiO_3 - LaMnO_3$ superlattices, Phys. Rev. B **87**, 195116 (2013).

[34] X. F. Zhai, L. Cheng, Y. Liu, C. M. Schlepütz, S. Dong, H. Li, X. Q. Zhang, S. Q. Chu, L. R. Zheng, J. Zhang, A. D. Zhao, H. Hong, A. Bhattacharya, J. N. Eckstein, and C. G. Zeng, Correlating interfacial octahedral rotations with magnetism in $(LaMnO_{3+\delta})_N/(SrTiO_3)_N$ superlattices, Nat. Commun. **5**, 4238 (2014).

[35] C. Ritter, M. R. Ibarra, J. M. De Teresa, P. A. Algarabel, C. Marquina, J. Blasco, J. García, S. Oseroff, and S.-W. Cheong, Influence of oxygen content on the structural, magnetotransport, and magnetic properties of $LaMnO_{3+\delta}$, Phys. Rev. B **56**, 8902 (1997).

[36] W. S. Choi, Z. Marton, S. Y. Jang, S. J. Moon, B. C. Jeon, J. H. Shin, S. S. A. Seo, T. W. Noh, K. Myung-Whun, H. N. Lee, and Y. S. Lee, Effects of oxygen-reducing atmosphere annealing on $LaMnO_3$ epitaxial thin films, J. Phys. D **42**, 165401 (2009).

[37] P. Orgiani, C. Aruta, R. Ciancio, A. Galdi, and L. Maritato, En-hanced transport properties in $La_xMnO_{3-\delta}$ thin films epitaxially

grown on $SrTiO_3$ substrates: The profound impact of the oxygen content, Appl. Phys. Lett. **95**, 013510 (2009).

[38] Y. S. Hou, H. J. Xiang, and X. G. Gong, Intrinsic insulating ferromagnetism in manganese oxide thin films, Phys. Rev. B **89**, 064415 (2014).

[39] J. H. Lee, K. T. Delaney, E. Bousquet, N. A. Spaldin, and K. M. Rabe, Strong coupling of Jahn-Teller distortion to oxygen-octahedron rotation and functional properties in epitaxially strained orthorhombic $LaMnO_3$, Phys. Rev. B **88**, 174426 (2013).

[40] B. R. K. Nanda and S. Satpathy, Density functional studies of $LaMnO_3$ under uniaxial strain, J. Magn. Magn. Mater. **322**, 3653 (2010).

[41] T. Hotta, Existence of a metallic ferromagnetic phase in models for undoped manganites, Phys. Rev. B **67**, 104428 (2003).

[42] X. R. Wang, C. J. Li, W. M. Lü, T. R. Paudel, D. P. Leusink, M. Hoek, N. Poccia, A. Vailionis, T. Venkatesan, J. M. D. Coey, E. Y. Tsymbal, Ariando, and H. Hilgenkamp, Imaging and control of ferromagnetism in $LaMnO_3/SrTiO_3$ heterostructures, Science **349**, 716 (2015).

[43] N. Nakagawa, H. Y. Hwang, and D. A. Muller, Why some interfaces cannot be sharp, Nat. Mater. **5**, 204 (2006).

[44] P. Delugas, A. Filippetti, V. Fiorentini, D. I. Bilc, D. Fontaine, and P. Ghosez, Spontaneous 2-Dimensional Carrier Confine-ment at the n-type $SrTiO_3/LaAlO_3$ Interface, Phys. Rev. Lett. **106**, 166807 (2011).

[45] H. H. Chen, A. M. Kolpak, and S. Ismail-Beigi, Electronic and magnetic properties of $SrTiO_3/LaAlO_3$ interfaces from first principles, Adv. Mater. **22**, 2881 (2010).

[46] J. Z. Sun, D. W. Abraham, R. A. Rao, and C. B. Eom, Thickness-dependent magnetotransport in ultrathin manganite films, Appl. Phys. Lett. **74**, 3017 (1999).

[47] R. P. Borges, W. Guichard, J. G. Lunney, J. M. D. Coey, and F. Ott, Magnetic and electric "dead" layers in $(La_{0.7}Sr_{0.3})MnO_3$ thin films, J. Appl. Phys. **89**, 3868 (2001).

[48] J. J. Kavich, M. P. Warusawithana, J. W. Freeland, P. Ryan, X. Zhai, R. H. Kodama, and J. N. Eckstein, Nanoscale suppression of magnetization at atomically assembled manganite interfaces: XMCD and XRMS measurements, Phys. Rev. B **76**, 014410 (2007).

[49] M. Huijben, L. W. Martin, Y.-H. Chu, M. B. Holcomb, P. Yu, G. Rijnders, D. H. A. Blank, and R. Ramesh, Critical thickness and orbital ordering in ultrathin $La_{0.7} Sr_{0.3} MnO_3$ films, Phys. Rev. B **78**, 094413 (2008).

[50] A. Tebano, C. Aruta, S. Sanna, P. G. Medaglia, G. Balestrino, A. A. Sidorenko, R. De Renzi, G. Ghiringhelli, L. Braicovich, V. Bisogni, and N. B. Brookes, Evidence of Orbital Reconstruction at Interfaces in Ultrathin $La_{0.67} Sr_{0.33} MnO_3$ Films, Phys. Rev. Lett. **100**, 137401 (2008).

[51] L. F. Kourkoutis, J. H. Song, H. Y. Hwang, and D. A. Muller, Microscopic origins for stabilizing room-temperature ferromagnetism in ultrathin manganite layers, Proc. Natl. Acad. Sci. USA **107**, 11682 (2010).

[52] A. X. Gray, C. Papp, B. Balke, S.-H. Yang, M. Huijben, E. Rotenberg, A. Bostwick, S. Ueda, Y. Yamashita, K. Kobayashi, E. M. Gullikson, J. B. Kortright, F. M. F. de Groot, G. Rijnders, D. H. A. Blank, R. Ramesh, and C. S. Fadley, Interface properties of magnetic tunnel junction $La_{0.7} Sr_{0.3} MnO_3/SrTiO_3$ superlattices studied by standing-wave excited photoemission spectroscopy, Phys. Rev. B **82**, 205116 (2010).

[53] F. Song, Å. F. Monsen, Z. S. Li, J. W. Wells, and E. Wahlström, The layer-by-layer stoichiometry of $La_{0.7}Sr_{0.3}MnO_3/SrTiO_3$ thin films and interfaces, Surf. Interface Anal. **45**, 1144 (2013).

[54] R. Peng, H. C. Xu, M. Xia, J. F. Zhao, X. Xie, D. F. Xu, B. P. Xie, and D. L. Feng, The origin of the dead-layer at the $La_{0.67} Sr_{0.33} MnO_3/SrTiO_3$ interface and dead-layer reduction via interfacial engineering, Appl. Phys. Lett. **104**, 081606 (2014).

[55] J. Xia, W. Siemons, G. Koster, M. R. Beasley, and A. Kapitulnik, Critical thickness for itinerant ferromagnetism in ultrathin films of $SrRuO_3$, Phys. Rev. B **79**, 140407(R) (2009).

[56] Y. J. Chang, C. H. Kim, S.-H. Phark, Y. S. Kim, J. Yu, and T. W. Noh, Fundamental Thickness Limit of Itinerant Ferromagnetic $SrRuO_3$ Thin Films, Phys. Rev. Lett. **103**, 057201 (2009).

[57] J. Jilili, F. Cossu, and U. Schwingenschlögl, Trends in $(LaMnO_3)_n/(SrTiO_3)_m$ superlattices with varying layer thicknesses, Sci. Rep. **5**, 13762 (2015).

[58] H. M. Liu, C. Y. Ma, P. X. Zhou, S. Dong, and J.-M. Liu, Magnetic orders and electronic structure in $LaMnO_3/SrTiO_3$ superlattices, J. Appl. Phys. **113**, 17D902 (2013).

[59] See Supplemental Material at http://link.aps.org/supplemental/10.1103/PhysRevB.96.235112 for more details of methods and other results on low U_{eff}'s.

[60] J. P. Perdew, K. Burke, and M. Ernzerhof, Generalized Gradient Approximation Made Simple, Phys. Rev. Lett. **77**, 3865 (1996).

[61] J. P. Perdew, J. A. Chevary, S. H. Vosko, K. A. Jackson, M. R. Pederson, D. J. Singh, and C. Fiolhais, Atoms, molecules, solids, and surfaces: Applications of the generalized gradient approximation for exchange and correlation, Phys. Rev. B **46**, 6671 (1992).

[62] P. E. Blöchl, Projector augmented-wave method, Phys. Rev. B **50**, 17953 (1994).

[63] G. Kresse and J. Furthmüller, Efficient iterative schemes for ab initio total-energy calculations using a plane-wave basis set, Phys. Rev. B **54**, 11169 (1996).

[64] G. Kresse and D. Joubert, From ultrasoft pseudopotentials to the projector augmented-wave method, Phys. Rev. B **59**, 1758 (1999).

[65] H. Sawada, Y. Morikawa, K. Terakura, and N. Hamada, Jahn-Teller distortion and magnetic structures in $LaMnO_3$, Phys. Rev. B **56**, 12154 (1997).

[66] T. Hashimoto, S. Ishibashi, and K. Terakura, Jahn-Teller distortion and magnetic structure in $LaMnO_3$: A first-principles theoretical study with full structure optimizations, Phys. Rev. B **82**, 045124 (2010).

[67] W.-C. Lee and A. H. MacDonald, Modulation doping near Mott-insulator heterojunctions, Phys. Rev. B **74**, 075106 (2006).

[68] T. A. Mellan, F. Corà, R. Grau-Crespo, and S. Ismail-Beigi, Importance of anisotropic coulomb interaction in $LaMnO_3$, Phys. Rev. B **92**, 085151 (2015).

[69] P. Rivero, V. Meunier, and W. Shelton, Electronic, structural, and magnetic properties of $LaMnO_3$ phase transition at high temperature, Phys. Rev. B **93**, 024111 (2016).

[70] S. L. Dudarev, G. A. Botton, S. Y. Savrasov, C. J. Humphreys, and A. P. Sutton, Electron-energy-loss spectra and the structural stability of nickel oxide: An LSDA+U study, Phys. Rev. B **57**, 1505 (1998).

[71] A. I. Liechtenstein, V. I. Anisimov, and J. Zaanen, Density-functional theory and strong interactions: Orbital ordering in Mott-Hubbard insulators, Phys. Rev. B **52**, R5467 (1995).

[72] J. P. Perdew, A. Ruzsinszky, G. I. Csonka, O. A. Vydrov, G. E. Scuseria, L. A. Constantin, X. L. Zhou, and K. Burke, Restoring the Density-Gradient Expansion for Exchange in Solids and Surfaces, Phys. Rev. Lett. **100**, 136406 (2008).

[73] T. Arima, Y. Tokura, and J. B. Torrance, Variation of optical gaps in perovskite-type $3d$ transition-metal oxides, Phys. Rev. B **48**, 17006 (1993).

[74] T. Saitoh, A. E. Bocquet, T. Mizokawa, H. Namatame, A. Fujimori, M. Abbate, Y. Takeda, and M. Takano, Electronic structure of $La_{1-x}Sr_xMnO_3$ studied by photoemission and x-ray-absorption spectroscopy, Phys. Rev. B **51**, 13942 (1995).

[75] J. H. Jung, K. H. Kim, D. J. Eom, T. W. Noh, E. J. Choi, Jaejun Yu, Y. S. Kwon, and Y. Chung, Determination of electronic band structures of $CaMnO_3$ and $LaMnO_3$ using optical-conductivity analyses, Phys. Rev. B **55**, 15489 (1997).

[76] W. Siemons, G. Koster, H. Yamamoto, W. A. Harrison, G. Lucovsky, T. H. Geballe, D. H. A. Blank, and M. R. Beasley, Origin of Charge Density at $LaAlO_3$ on $SrTiO_3$ Heterointerfaces: Possibility of Intrinsic Doping, Phys. Rev. Lett. **98**, 196802 (2007).

[77] M. Basletic, J.-L. Maurice, C. Carrétéro, G. Herranz, O. Copie, M. Bibes, É. Jacquet, K. Bouzehouane, S. Fusil, and A. Barthélémy, Mapping the spatial distribution of charge carriers in $LaAlO_3/SrTiO_3$ heterostructures, Nat. Mater. **7**, 621 (2008).

[78] U. Aschauer, R. Pfenninger, S. M. Selbach, T. Grande, and N. A. Spaldin, Strain-controlled oxygen vacancy formation and ordering in $CaMnO_3$, Phys. Rev. B **88**, 054111 (2013).

[79] C. Cen, S. Thiel, G. Hammerl, C. W. Schneider, K. E. Andersen, C. S. Hellberg, J. Mannhart, and J. Levy, Nanoscale control of an interfacial metal-insulator transition at room temperature, Nat. Mater. **7**, 298 (2008).

[80] Z. C. Zhong, P. X. Xu, and P. J. Kelly, Polarity-induced oxygen vacancies at $LaAlO_3/SrTiO_3$ interfaces, Phys. Rev. B **82**, 165127 (2010).

[81] W.-J. Son, E. Cho, B. Lee, J. Lee, and S. Han, Density and spatial distribution of charge carriers in the intrinsic n-type $LaAlO_3$-$SrTiO_3$ interface, Phys. Rev. B **79**, 245411 (2009).

[82] M. J. Calderón, L. Brey, and F. Guinea, Surface electronic structure and magnetic properties of doped manganites, Phys. Rev. B **60**, 6698 (1999).

[83] H. W. Guo, Z. Wang, S. Dong, S. Ghosh, M. Saghayezhian, L. N. Chen, Y. K. Weng, A. Herklotz, T. Z. Ward, R. Y. Jin, S. T. Pantelides, Y. M. Zhu, J. D. Zhang, and E. W. Plummer, Interface-induced multiferroism by design in complex oxide superlattices, Proc. Natl. Acad. Sci. USA **114**, E5062 (2017).

[84] J. D. Burton and E. Y. Tsymbal, Prediction of electrically induced magnetic reconstruction at the manganite/ferroelectric interface, Phys. Rev. B **80**, 174406 (2009).

[85] Z. Liao, M. Huijben, Z. Zhong, N. Gauquelin, S. Macke, R. J. Green, S. Van Aert, J. Verbeeck, G. Van Tendeloo, K. Held, G. A. Sawatzky, G. Koster, and G. Rijnders, Controlled lateral anisotropy in correlated manganite heterostructures by interface-engineered oxygen octahedral coupling, Nat. Mater. **15**, 425 (2016).

[86] J. B. Goodenough, Theory of the role of covalence in the perovskite-type manganites [La,M(II)]MnO_3, Phys. Rev. **100**, 564 (1955).